International Journal of Greenhouse Gas Control 106 (2021) 103225

Contents lists available at ScienceDirect

International Journal of Greenhouse Gas Control

journal homepage: www.elsevier.com/locate/ijggc

Experimental assessment of the hydro-mechanical behaviour of a shale caprock during CO_2 injection

Alberto Minardi [a], Eleni Stavropoulou [a,*], Taeheon Kim [a], Alessio Ferrari [a,b], Lyesse Laloui [a]

[a] Ecole Polytechnique Fédérale de Lausanne (EPFL), Laboratory for Soil Mechanics (LMS), EPFL-ENAC-LMS, Station 18, Lausanne, CH-1015, Switzerland
[b] Università degli Studi di Palermo, Engineering Department Viale delle Scienze, edificio 8, Palermo, 90128, Italy

ARTICLE INFO

Keywords:
Geological CO_2 sequestration
Shales
Opalinus Clay
Capillary entry-pressure
Caprock integrity

ABSTRACT

The presented experimental study focuses on the hydro-mechanical characterisation of a shale caprock (Opalinus Clay) in contact with carbon dioxide. The objective of this paper, consists in the evaluation of the material's sealing capacity in terms of entry-pressure, mechanical behaviour and sensitivity of the transport properties to chemo-mechanical effects induced by gaseous and liquid CO_2 injection. Two types of Opalinus Clay core samples are tested; shaly and carbonate-rich. The sealing capacity has been evaluated on the shaly OPA according to the stepwise and the residual methods and compared to the results from mercury intrusion porosimetry. The obtained results and the differences associated to the different involved physical processes are discussed and compared with literature data. Injection tests carried out in saturated and unsaturated conditions have revealed that sub-critical CO_2 propagation in a water saturated material is not associated with generation of fractures. On the other hand, the generation of capillary forces is affecting the mechanical behaviour beside the sealing capacity. The impact of chemical effects on the permeability of both types of OPA is analysed with long-term CO_2 injection tests, where no significant variations of permeability are measured during the exposure time investigated. The challenges related to this type of analysis with laboratory scale experiments are illustrated and new insights on the behaviour of Opalinus Clay when subjected to injection of a non-wetting fluid are highlighted.

1. Introduction

Carbon capture and storage (CCS) is widely recognised to have great potential for sustainable and environmentally friendly energy production. In carbon geosequestration, CO_2 is captured from large emitters, purified, compressed and injected in deep reservoir formations of high porosity. Structural trapping, where a caprock acts as a sealing barrier to the CO_2 migration and leakage (Wollenweber et al., 2010; Armitage et al., 2013), is the primary sequestration mechanism during at least the first decades and thus, sequestration efficiency relies on the sealing properties of the caprock.

Rock formations with low porosity are commonly identified caprocks for CO_2 sequestration, as it is assumed that because of their small pores, high capillary forces are created preventing the CO_2 from entering the caprock (Hesse et al., 2008; Espinoza and Santamarina, 2017). Shales and more in general argillaceous rocks are known to present favourable hydro-mechanical properties, such as low permeability, high sorption capacity, high swelling ability and high capillary entry pressure.

The sealing capacity of a geomaterial is usually quantified based on its measured capillary entry-pressure. The capillary entry-pressure is the maximum pressure difference that may exist across the interface that separates two immiscible fluids before the non-wetting fluid penetrates the pore space. It is calculated as the pressure of the non-wetting phase (here, CO_2) minus the pressure of the wetting phase (here, pore fluid) (Iglauer et al., 2015). The wettability depends on its surface tension, *i.e.* the intermolecular forces that result in minimising the interfacial areas between the different existing phases, and it is determined by the contact angle of the fluid.

The capillary entry-pressure can be evaluated either with direct laboratory scale injection tests or with indirect methodologies that are typically based on the evaluation of the material's pore size (*e.g.* with mercury intrusion porosimetry test), wettability and mineralogical composition (Iglauer et al., 2015; Chiquet et al., 2007a). These indirect methodologies are usually considered to be able to provide a preliminary evaluation of the sealing capacity of geomaterials; however, they are limited by the testing conditions (boundary stress conditions and sample size), calling into question the consistency of the determined capillary entry-pressure. Direct CO_2 injection testing can provide a more

* Corresponding author.
E-mail address: eleni.stavropoulou@epfl.ch (E. Stavropoulou).

https://doi.org/10.1016/j.ijggc.2020.103225
Received 29 May 2020; Received in revised form 27 November 2020; Accepted 1 December 2020
Available online 19 January 2021

reliable assessment of the capillary entry-pressure. The step by step approach is identified as the main technique for the identification of the capillary-entry pressure, however, an accurate evaluation in low-permeability materials according to this method can be a very long and challenging process (Busch and Müller, 2011). Other methods have been investigated in literature, such as dynamic, racking or residual pressure methods (Wollenweber et al., 2010; Egermann et al., 2006). As further detailed by Boulin et al. (2013), each method presents advantages and limitations related to accuracy, duration and representative of the *in-situ* conditions stress-wise and in terms of fluid migration.

Together with the hydro-mechanical properties of the caprock, chemical interactions between the caprock and CO_2 play a key role to the sealing capacity and integrity. The injection of CO_2 in water-saturated geomaterials might induce minerals dissolution and precipitation processes. As the injected CO_2 dissolves in the pore fluid, part of it generates carbonic acid (H_2CO_3) through the following reactions (Rosenbauer et al., 2005):

$$\begin{aligned} &CO_{2_{(aq)}} + H_2O_{(l)} \leftrightarrow H_2CO_{3_{(aq)}} \\ &H_2CO_{3_{(aq)}} \leftrightarrow H^+_{(aq)} + HCO3^-_{3_{(aq)}} \\ &HCO^-_{3_{(aq)}} \leftrightarrow H^+_{(aq)} + CO^{2-}_{3_{(aq)}} \end{aligned} \quad (1)$$

The presence of carbonic acid causes a decrease of the pH of the fluid, causing an alteration of the *in-situ* chemical equilibrium. The mineralogical alteration process and the induced geomechanical response depend on the resident material. More precisely, silicate minerals are initially dissolved by carbonic acid releasing divalent cations (Ca^+_2, Mg^+_2, *etc.*), and later the released cations react with carbonate ions forming carbonate crystals and secondary silicate minerals (Rosenbauer et al., 2005). On the other hand, pre-existing carbonate crystals might be dissolved by the acidic fluid until chemical equilibrium is reached. Such geochemical alterations tend to modify the transport properties (Busch et al., 2008).

Mineral alteration can cause microstructural changes that might reflect in basic properties of the material such as porosity and premeability. Unless the capillary entry-pressure is exceeded, the injected CO_2 can migrate in the caprock's pore system only by diffusion. Given the slow dissolution kinetics and the very low permeability of shales, the observation of significant alterations is difficult, even in the presence of faster reactive phases such as carbonates (Palandri and Kharaka, 2004). Caprock formations that show low reactivity to carbonic acid and are therefore capable of maintaining their integrity at low pH conditions are obviously preferred for geological CO_2 sequestration.

In Switzerland, the Opalinus Clay is considered as a reference caprock-like formation for possible carbon geosequestration. This overconsolidated shale formation is composed by 40–80% clay minerals and micas, 10–40% quartz, 5–40% calcite, 1–5% siderite, 0–1.7% pyrite and 0.1–0.5% organic carbon (Bossart and Thury, 2008). The anisotropy of Opalinus Clay has been studied by several authors (Bossart and Thury, 2008; Salager et al., 2013; Favero et al., 2018), and it has been found to reflect in main hydro-mechanical properties of the material, such as stiffness, swelling behaviour, and permeability. Other authors have investigated the hydro-mechanical behaviour of Opalinus Clay pointing out its sensitivity to water content variations in terms of stiffness, volumetric changes or shear strength parameters (Ferrari et al., 2014; Crisci et al., 2019; Orellana et al., 2018). The mineralogical composition of Opalinus Clay can also affect the material's response, the strength and rigidity of which have been found higher for higher quartz and carbonate content (Minardi et al., 2016). The low permeability (in the order of nano Darcy), the low porosity (lower than 20%) and modal pore size (nano meter range), and the high clay content make the Opalinus Clay a good formation to be employed as a barrier material (Marschall et al., 2005) for the sequestration of CO_2. Indeed, these features are essential for a high sealing capacity and low sensitivity of the hydro-mechanical properties to chemical effects.

Despite the large potential of the Opalinus Clay formation for the sequestration of CO_2 (Chevalier et al., 2010), geomechanical characterisation of the material involving CO_2 is limited. The goal of this experimental work is twofold aiming to deepen the current knowledge on the possible use of the Opalinus Clay formation as a caprock for CO_2 storage. The first objective is a deep evaluation of the sealing capacity of the Opalinus Clay, not simply by measuring the capillary-entry pressure, but also with the analysis of the mechanical response experienced by the material during the injection of CO_2. Indeed, a full understanding of the hydro-mechanical response during the injection is fundamental to better analyse the transport mechanisms that dominate the CO_2 flow in the fluid saturated geomaterial. The second objective is the investigation of the influence of the CO_2 on the permeability of the material, where different treatment methodologies are considered. In addition, the possible chemical effect induced by the exposure to an acidic fluid is also analysed by means of pore size distribution and grain density analysis.

To achieve these objectives, CO_2 injection tests are performed at the laboratory scale under different levels of injection pressure and different durations. CO_2 is injected under ambient temperature conditions, *i.e.* under sub-critical conditions. Even though *in-situ* storage conditions often involve super-critical CO_2 (elevated pressure and temperature), the sub-critical testing conditions of the current case study can be attributed in realistic off-shore storage conditions, where CO_2 is transported and injected in liquid state (McCoy and Rubin, 2008; Vilarrasa et al., 2013). Besides, as further explained later in the paper, the applied test conditions aim to reproduce a similar configuration with a large-scale *in-situ* experiment in Mont-Terri underground laboratory where CO_2-rich crine is injected in Opalinus Clay (Zappone et al., 2018).

Taking into account the variability of the mineralogical composition, two different facies are tested: shaly and carbonate-rich Opalinus Clay. The details of the tested materials are illustrated in the next section, followed by the adopted testing procedure to carry out the experiments. The obtained results are then presented in the second part of the article.

2. Tested material

Opalinus Clay (OPA) core samples collected from the Mont Terri Underground Research Laboratory (Switzerland) have been used for the experimental activities. Three different lithofacies are identified in the Mont Terri underground laboratory (Bossart and Thury, 2008), wherefrom the studied core samples originate: in the lower part a shaly facies, an interstratified sandy and shaly facies in the upper part and a sandy-limy facies in between. The samples tested in the presented experimental study have been obtained from two different core samples: (i) a clay-rich core sample extracted at the connection between the gallery 08 and the niche DR-A in the shaly facies, and (ii) a carbonate-rich core sample extracted form the niche 08 at the edge between the shaly and the carbonate units. The first core sample exhibits a rather homogeneous composition dominated by clay particles. The second core sample is more heterogeneous due to presence of carbonate lenses. This carbonate-rich zone of the second core sample has been used for the preparation of a carbonate-rich sample. Fig. 1 highlights the difference between the two materials, where the carbonate-rich material (Fig. 1b) presents a more pronounced heterogeneity than the clay-rich material (Fig. 1a). These aspects are confirmed by the mineralogical composition of the two materials (Table 1), where the different amount of carbonate and clay minerals is quantified.

The properties of each core sample have been measured. First, the grain density (ρ_s) is obtained with the water pycnometer technique (ASTM, 2010) on material crushed and sieved at 0.5 mm. A value of $\rho_{s,sh} = 2.75\ g/cm^3$ is obtained for the shaly OPA, while for the carbonate-rich OPA a lower grain density value $\rho_{s,c} = 2.67\ g/cm^3$ is measured. This density difference is due to the difference in mineralogical composition between the two types Opalinus Clay (Rieke and Chilingarian, 1974). The bulk density (ρ) of the core sample is measured based on the fluid displacement technique on a slice from which the samples are prepared. For the shaly OPA core sample, $\rho_{sh} = 2.35\ g/cm^3$

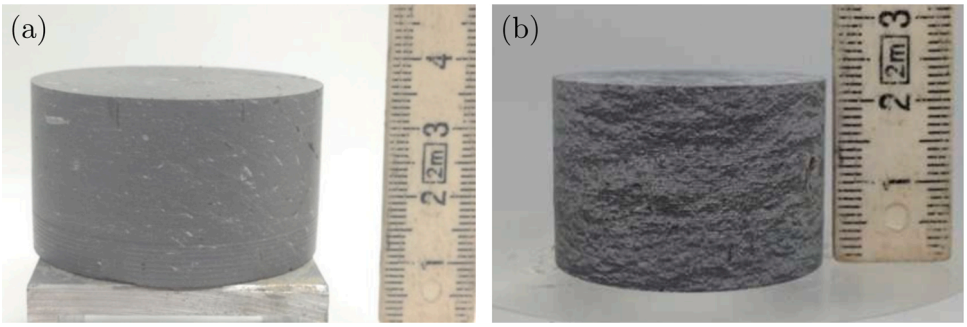

Fig. 1. Example of tested materials: (a) shaly Opalinus Clay, (b) carbonate-rich Opalinus Clay.

Table 1
Mineralogical composition of the two core samples used for the experimental investigation.

(wt%)	Quartz	Carbonate	Clay	Other
Shaly OPA	6	20	68	6
Carbonate-rich OPA	8	50	37	5

and for the carbonate-rich OPA core sample, $\rho_c = 2.53$ g/cm^3. Finally the water content (w) is obtained from oven-drying at 110 °C and is calculated for the shaly OPA core sample $w_{sh} = 3.9\%$, while for the carbonate-rich OPA core sample $w_c = 3.7\%$. The void ratio can be finally calculated, corresponding to a higher value for the shaly OPA ($e = 0.22$) than the carbonate-rich OPA ($e = 0.095$).

The pore structure of the two different types of Opalinus Clay (shaly and carbonate-rich) is studied with Mercury Intrusion Porosimetry (MIP) tests, where the freeze-drying technique is adopted for the samples' preparation. The results of the performed tests are plotted in Fig. 2 and reveal a different type of pore size distribution (PSD) for each type of Opalinus Clay; a unimodal distribution is obtained for the shaly OPA (Fig. 2a), while a bimodal distribution is exhibited by the carbonate-rich OPA (Fig. 2b). The peak observed at the low pore diameters (10–30 nm) is consistent for both types of samples and it corresponds to the presence of pores in the clay matrix of the specimen. Similar results with dominant pore size in the order of 10–30 nm are presented in Favero et al. (2018). Slightly lower dominant pore size (lower than 10 nm) have been highlighted in Amann-Hildenbrand et al. (2015) and Busch et al. (2017). The second peak of the carbonate-rich sample at the higher range of pore diameters (between 10 μm and 100 μm) might be related to the presence of micro-fissures in the material, in particular at the interface between the carbonate and the clay particles.

3. Experimental campaign

3.1. Testing device

A high pressure oedometric cell (Ferrari et al., 2016) is used to perform the CO_2 injection tests (Fig. 3). This device allows the testing of samples with 12.5 mm and 35.0 mm height and diameter, respectively. The preparation of the samples is done with a mechanical lathe by reducing the size of a slice of material obtained from the core sample. After preparation, the samples are recored with the oedometric ring, ensuring the lateral contact between the material and the ring. Different pumps are connected to the oedometric cell allowing the possibility to inject different types of fluid. As illustrated in Fig. 3, water can be injected at both sides of the sample (upstream and downstream); two different pumps are used to control pressure up to 16 MPa and volume with a resolution of 1 mm^3. A third pump connected to the upstream side is used to inject CO_2 (both gas and liquid state) with a range up to 25 MPa and a volume resolution of 1 mm^3. Two pressure transducers are also mounted on the pore fluid lines at the two sides of the sample to monitor the fluid pressures when the pumps are disconnected from the cell (external valves are closed). The axial stress is applied with a hydraulic jack that allows the application of a maximum total vertical stress equal to 100 MPa. The vertical displacements are measured by three LVDTs (resolution of 0.2 μm), which measure the relative displacement of the cell with respect to the piston. The deformation of the testing device has been carefully assessed during a preliminary calibration using a dummy metallic sample, the mechanical behaviour of which is known.

In the following sections, two main sets of experiments are presented in detail along with the corresponding testing methodologies. First, a series of short-term injection tests on the shaly OPA performed for the evaluation of the sealing capacity in terms of capillary entry-pressure are

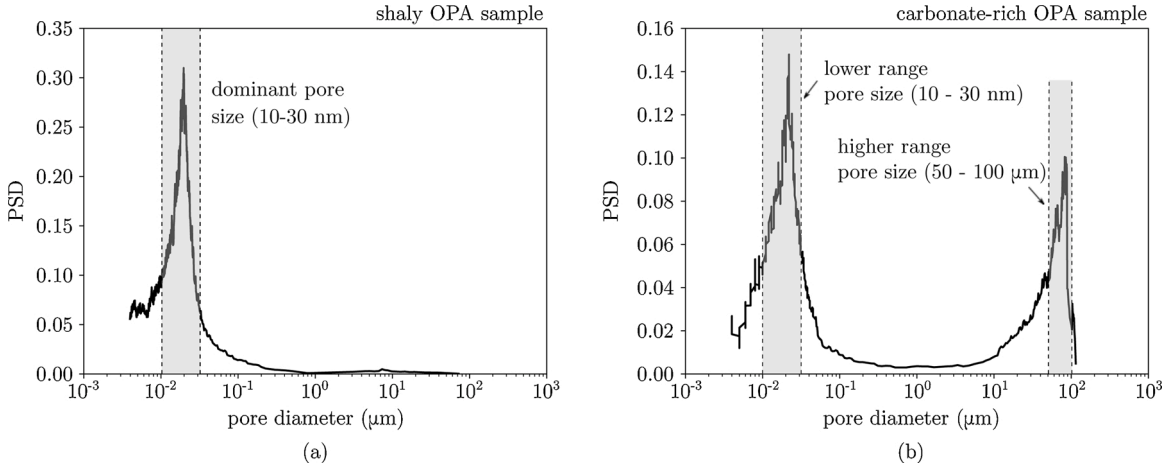

Fig. 2. Pore size distribution of (a) shaly OPA sample and (b) a carbonate-rich OPA sample.

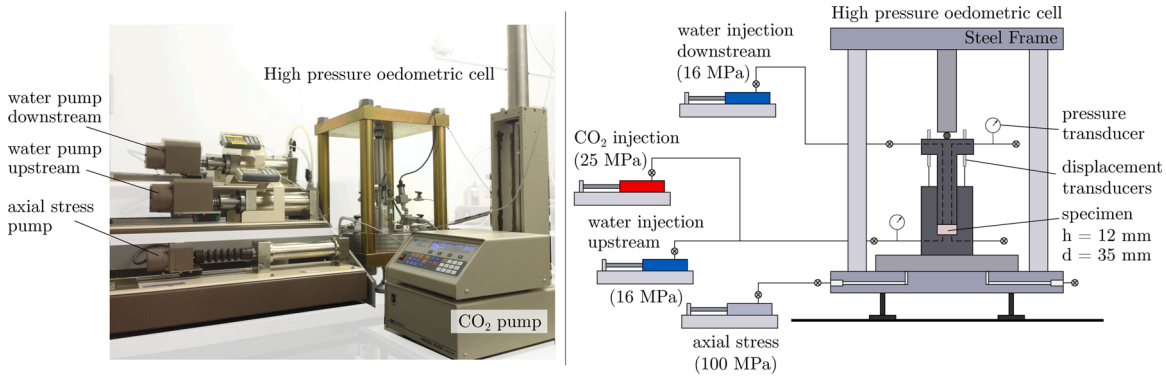

Fig. 3. Testing layout of the oedometric set-up used in the experimental campaign.

presented. Afterwards, two long-term CO_2 injection tests are presented for the investigation of the chemical impact on the material's transport properties: one on the carbonate-rich OPA and one on the shaly OPA. Both sets of experiments – short- and long-term, shaly and carbonate OPA – are divided in two main phases: pre-exposure (resaturation and consolidation phase), CO_2 injection phase.

The tests are carried out at standard laboratory temperature, *i.e.* 21 °C. The applied boundary conditions (pressure and temperature) aim to achieve a similar configuration with the *in-situ* experiment carried out in the Mont Terri underground laboratory (Zappone et al., 2018) from where the studied cores are extracted. Moreover, in the frame of the hydro-mechanical analysis of the material with CO_2 injection, the use of liquid CO_2 is preferred to supercritical in order to avoid additional mechanical implications introduced with the increase of temperature (Favero et al., 2016a).

Finally, for the analysis of the results, it is worthy taking into account the impact of the pressure and temperature level to the surface tension and contact angle and consequently to the value of entry-pressure, as pointed out by various authors (Iglauer et al., 2015; Chiquet et al., 2007a,b; Kaveh et al., 2016; Favero and Laloui, 2018); higher pressure leads to lower surface tension and higher contact angle (θ), resulting in lower entry pressure. Even though, the change of contact angle with temperature is less significant at higher pressures (Kaveh et al., 2016), the effect of temperature on interfacial tension between CO_2 and water cannot be neglected for CO_2 storage analysis. Indeed, Iglauer et al. (2015) pointed out that for structural trapping, lower caprock wettability with increasing pressure or temperature can be attributed to a lower storage capacity. In the experimental setup of the currently presented work, CO_2 is injected in liquid state at a pressure past the critical point, therefore the obtained results are not directly applicable to super-critical *in-situ* storage conditions. However, liquid CO_2 injection is not uncommon, for example in offshore storage cases where cold CO_2 is injected (Hansen et al., 2013).

3.2. Short-term injection testing: capillary entry-pressure assessment

A sample from the shaly OPA core is used for the study of the material's capillary-entry pressure. The sample's properties are measured before the testing; bulk density $\rho = 2.32$ g/cm^3, water content w = 1.9%, void ratio e = 0.21.

The preparation procedure dries out the sample, this is why the sample is first resaturated and loaded to the target effective axial stress. Afterwards, a first estimation of the entry-pressure is obtained with a short-duration CO_2 injection test in the saturated sample using the *stepwise* method. To highlight the importance of the initial saturation of the material for the assessment of the sealing capacity, an additional short-term injection test is performed on the same sample after having experienced a desaturation. In order to evaluate the consistency of the applied methodology, the saturated material's entry-pressure is also measured based on the *residual* method. The details of these two methodologies are presented in the next section.

3.2.1. Testing methodology

For the measurement of the material's entry-pressure, CO_2 is injected at the upstream side of the sample ($u_{CO_2}{}^{up}$), while on the downstream side either CO_2 ($u_{CO_2}{}^{dw}$) or water ($u_w{}^{up}$) can be used (Fig. 4). Different procedures can be adopted for the injection, either increasing the upstream CO_2 pressure with constant flow rate or with *stepwise* injection until CO_2 starts to be recovered in the downstream reservoir. The recovery of CO_2 at the downstream side indicates the occurrence of the breakthrough process.

At the downstream side, either constant volume or constant pressure conditions can be adopted in the reservoir. When constant pressure conditions are used (Fig. 4a), the outflow volume is monitored at the downstream side to assess to breakthrough of CO_2 across the sample. As illustrated in the graph of Fig. 4a, when an increase at the downstream outflow is observed (blue continuous plot), it is assumed that the capillary pressure of the material is exceeded and the injected CO_2 can flow through the sample. In the case of constant volume conditions (Fig. 4b), the breakthrough pressure is evaluated monitoring the evolution of the pressure in the downstream reservoir. Similarly, when a pressure increase at the downstream side is observed (orange plot), breakthrough of the capillary pressure is assumed. Furthermore, either water (Fig. 4a) or CO_2 (Fig. 4b) can be used at the downstream side; however, the use of water might lead to some difficulties in assessing the breakthrough process in low permeable geomaterials, such as shales, due to the diffusion of CO_2 in the pore fluid. A comprehensive review of the available experimental techniques to perform CO_2 injection tests can be found in Boulin et al. (2013), Makhnenko et al. (2017).

When a flow or pressure variation is observed at the downstream side, the corresponding pressure difference between the injected CO_2 and the water in the material's pore space is considered as the *breakthrough entry-pressure*, PE (Boulin et al., 2013). This pressure (PE) is generally higher than the capillary entry-pressure (P_c) in low permeable geomaterials.

Indeed, once the CO_2 starts to penetrate the sample, the pore fluid has to be displaced under the influence of the capillary forces, and a given time has to be considered for its migration across the sample before reaching the downstream side. Thus, a stepwise injection is usually preferred when testing low permeable geomaterials such as shales in order to minimise the influence of this delay and reduce the difference between breakthrough and capillary entry-pressures.

The residual method (Wollenweber et al., 2010) represents a good alternative for this type of investigation. This method requires a fully saturated sample (generally with water) and the principle involves a very high instantaneous increase of the upstream injection pressure of the non-wetting fluid ($u_{CO_2}{}^{up}$) to a value at least twice as high as the expected PE (Fig. 5). At the downstream side, the pressure evolution

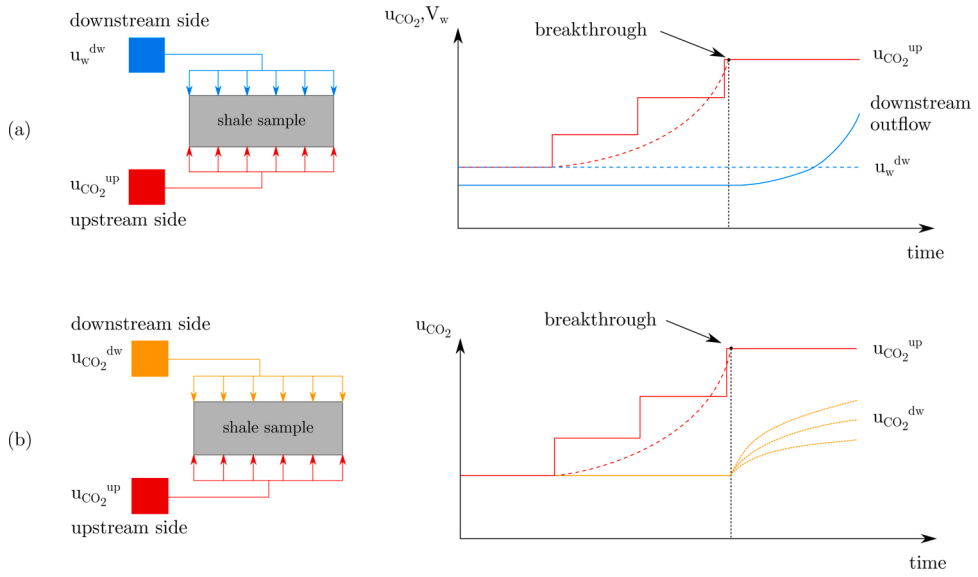

Fig. 4. Testing layout (left) and example of pressure-flow (right) during CO_2 injection tests with (a) constant pressure water reservoir, and (b) constant volume CO_2 reservoir at the downstream side. (For interpretation of the references to color in the text, the reader is referred to the web version of this article.).

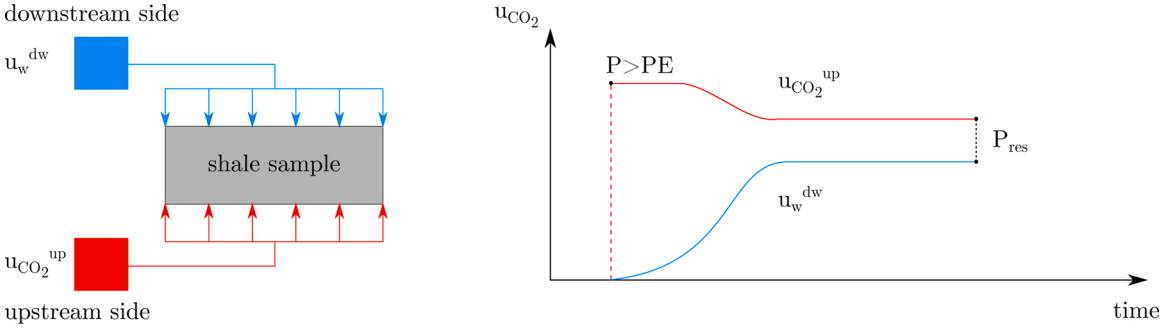

Fig. 5. Testing layout (left) and example of pressure evolution (right) during CO_2 injection tests according to the *residual* method.

($u_{w^{dw}}$) is monitored in a constant volume reservoir filled with water (wetting fluid).

Eventually, the CO_2 flows from the upstream to the downstream reservoir, causing a pressure decrease at the upstream side and a pressure increase at the downstream side, as illustrated in the graph of Fig. 18. When the downstream pressure is high enough, an imbibition process starts and stops the migration of the non-wetting fluid in the material. At this stage, a pressure difference between the two sides is exhibited, and it is called residual pressure. However, taking into account both the drainage and the imbibition processes, Zweigel et al. (2004) suggested that the residual pressure should be lower than the PE, confirmed later by Egermann et al. (2006). Pendland (2010) reported that the residual pressure is an intrinsic parameter of the tested material and corresponds to the *snap-off* pressure that indicates the reimbibition process; this process is different from an experiment for the measurement of the PE (Amann-Hildenbrand et al., 2012).

3.2.2. *Pre-exposure phase*

Before CO_2 injection, the shaly OPA sample is saturated with distilled de-aired water and progressively loaded to the target effective stress. It is assumed that given the shaly nature of the tested sample (low carbonate content), chemical activity (carbonate dissolution) is supposed to be negligible for the duration of the experiment. Fig. 6 shows the evolution of the total axial stress and water pressure in time, both upstream and downstream, during the first phase of the test. During the saturation, the sample is initially placed in contact with water at low pressure

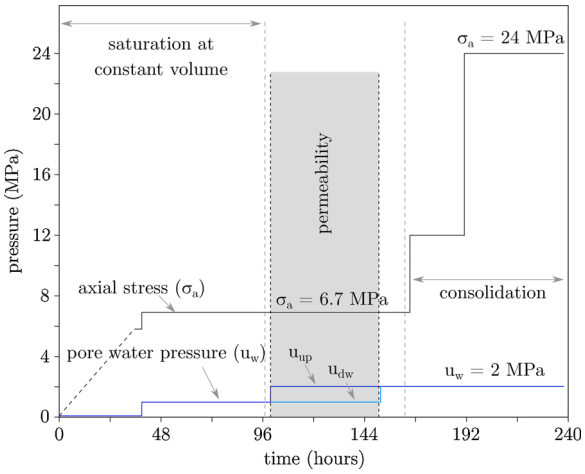

Fig. 6. Evolution of the total axial stress and fluid pressures during the pre-exposure phase of the test (saturation, permeability and consolidation) on the shaly OPA sample. (For interpretation of the references to color in the text, the reader is referred to the web version of this article.).

(<100 kPa – blue line) and the axial stress is progressively increased to keep constant volume conditions (dashed line). Once the stabilisation of the stress is achieved and the swelling stress is obtained, the water

pressure is increased to 1 MPa at both sides, while the total axial stress is also increased correspondingly to keep the effective stress constant. After a total of 4 days, the water pressure is increased to 2 MPa at the upstream side and maintained to 1 MPa at the downstream side for the measurement of the sample's hydraulic conductivity.

The saturation phase at constant volume has lasted for a period of 4 days, at the end of which a permeability measurement has taken place. At the end of the measurement the same water pressure (2 MPa) has been applied at both sides of the sample. The mechanical stress has then been increased in two steps to achieve the target effective stress (24 MPa of total axial stress), keeping the same water pressure at both sides of the sample equal to 2 MPa. The applied total axial stress corresponds to a depth of approximately 1000 m in the frame of CO_2 sequestration. From an experimental point of view, as the capillary entry-pressure is expected to be in the order of some MPas, this value of effective stress allows the application of a CO_2 injection pressure in the same order and therefore the investigation of a wide range of possible entry-pressure (from 1 MPa to 20 MPa).

The response of the sample during the initial saturation phase is presented in terms of axial strain, axial stress, and injected water volume in Fig. 7. The stabilisation of these quantities is used to assess the stabilisation of the swelling process. In Fig. 7a the evolution in time of the measured axial strain is plotted. The sample exhibits a stable condition after 24 h with a final expansion of −0.095%, which induced an increase of the void ratio of 0.001. Fig. 7b shows the evolution of the applied axial stress in time. A non-linear trend is observed, which indicates a more pronounced swelling response of the sample in the initial part of the saturation process. A final total axial swelling stress of 6 MPa is obtained. Finally, Fig. 7c shows the evolution of the injected water volume in time, measured from both sides of the sample. The observed stabilisation is a further indication that the saturation process reached a stable condition. However, the injected water volume (0.895 ml) has not been sufficient to fully saturate the sample. To further enhance the saturation, the water pressure has been increased to 1 MPa for about 4.5 days, as shown in Fig. 6 between the period of 36 and 96 h.

After saturation, the hydraulic conductivity of the sample is measured. The evaluation of the hydraulic conductivity is a good practice to assess the saturation level of the material before the injection of CO_2. Indeed, an incomplete saturation of the sample might affect significantly the evaluation of the sealing capacity and capillary entry-pressure of the material in the second phase of the test. A steady state methodology is adopted for the measurement, where a pressure difference of 1 MPa is applied between the upstream and downstream sides. More precisely, at the upstream side a water pressure of 2 MPa is applied, while a water pressure of 1 MPa is applied to the downstream side. A constant total axial stress equal to 6.7 MPa is constantly applied during the measurement. The inflow and outflow water volumes are monitored by the two water pumps at both sides. For the reported period of time, the hydraulic conductivity obtained from the outflow recorded at the downstream side is in the range 1–2 $\times 10^{-13}$ m/s and has to be referred to a void ratio of the material of 0.214. This range is consistent with other measurements performed on water saturated Opalinus Clay samples presented in Favero et al. (2016b).

3.2.3. CO_2 injection phase

After the end of the consolidation process, CO_2 injection is started. For the assessment of the capillary entry-pressure and the evaluation of the mechanical response of the material, CO_2 is injected in the saturated shaly OPA sample *stepwise* from the upstream side, as shown in Fig. 8. During the initial injection step (Step 0), the pore lines at both sides are flushed in order to replace the existing water with gaseous CO_2. The applied CO_2 pressure at this step is equal to the previous water pressure, *i.e.* 2 MPa, in order to keep the same boundary conditions while upstream and downstream sides are connected. Once a stable response is observed in terms of both displacement and pressure, the upstream and downstream sides are disconnected. CO_2 pressure is then increased at the upstream side only, while at the downstream side the pressure evolution is monitored in the constant volume reservoir with the pressure transducer. Unlike previous studies on the sealing capacity of caprock materials, in this work the mechanical response is also investigated along with the entry-pressure. To this end, larger pressure increments are adopted for a better evaluation of the sample's deformation during injection, which can still be considered acceptable for the evaluation of the hydraulic behaviour. More precisely, the pressure is increased in three steps from 2 MPa to 12 MPa, followed by a final step where the CO_2 pressure is decreased from 12 MPa to 8 MPa at the end of the short-term injection test. At each step the injection pressure is kept constant, and the pressure evolution at the downstream side and the sample response in terms of axial displacement are continuously monitored to assess the mechanical response and evaluate the capillary entry-pressure.

Fig. 8 shows the evolution of the CO_2 injection pressure in time at

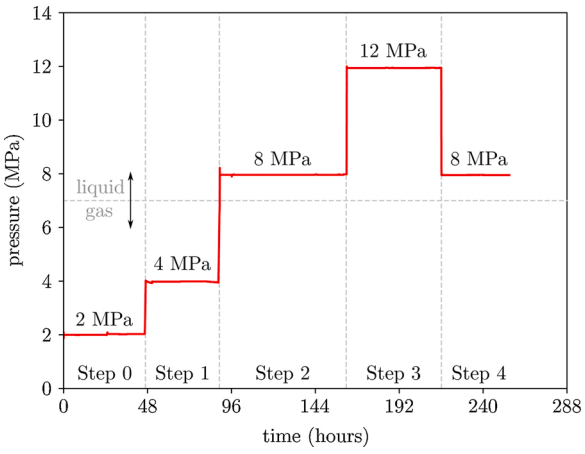

Fig. 8. Evolution in time of the CO_2 injection pressure at the upstream side during the injection phase of the test.

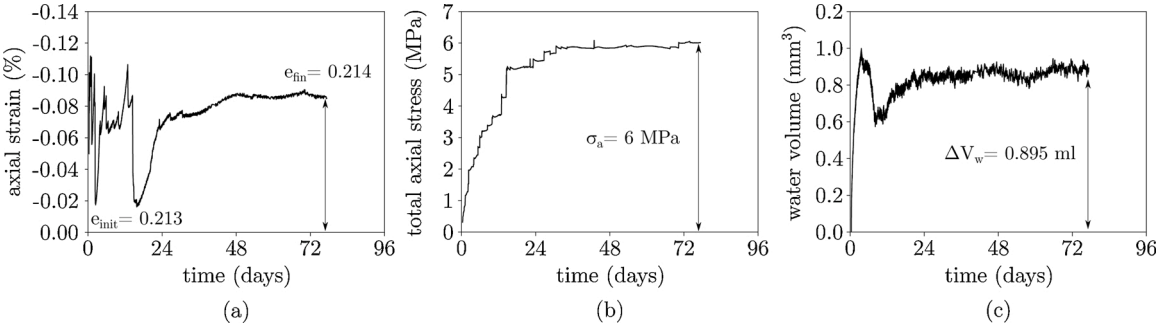

Fig. 7. Evolution in time of the (a) axial stain, (b) axial stress and (c) injected water volume during the initial saturation process at constant volume.

upstream side during a total time of 11 days. Evidently, the injected CO_2 is in gas phase during the first two steps (2 and 4 MPa), while during the higher applied pressure levels (8 and 12 MPa) the injected CO_2 is in liquid phase. At the end of the short-term CO_2 injection, the sample is dismounted from the cell, and it exhibited a water content equal to 8.0%, a degree of saturation equal to 82%, and a void ratio equal to 0.267.

In order to investigate the impact of water saturation on the sealing capacity of the material, a CO_2 injection test is performed on the same shaly sample in unsaturated conditions with the same injection protocol. Partial desaturation is not irrelevant to the *in-situ* conditions, as in particular cases such as during the drilling phase or on-field testing (*e.g.* Mont Terri) desaturation might occur. The sample is exposed to room temperature and pressure conditions for one month after the dismantling; after this period the water content has decreased to 3.1%, the void ratio to 0.235 (the drying process induced a shrinkage of the sample (Ferrari et al., 2014; Minardi et al., 2016)), and the water degree of saturation to 37%. Then, the sample is mounted in the cell and loaded to a total axial stress of 24 MPa without any water contact. The short-term CO_2 injection is then performed identically to the stepwise test previously presented; after the initial CO_2 injection to 2 MPa at both upstream and downstream sides, the injection pressure is increased in three steps (to 4, 8, and 12 MPa) at the upstream side, followed by a final decreasing step to 8 MPa (Fig. 8). Finally, the evaluation of the capillary-entry pressure with the residual method is performed. After the short-term injection in unsaturated conditions, the sample is resaturated applying a water pressure equal to 8 MPa at both upstream and downstream side and a total axial stress equal to 30 MPa. The injection of CO_2 is carried out at the upstream side by applying an instantaneous increase of pressure from 8 MPa to 16 MPa. Once the target pressure is achieved, the injection is stopped and constant volume reservoir conditions are applied at both sides of the sample, and the pressure evolution in time at the two sides is monitored until stabilisation is observed.

3.3. Long-term injection testing: transport properties evaluation

The objective of this long-term experimental campaign is the evaluation of the impact of the material's exposure to CO_2 on the permeability, which is a key parameter responsible for the integrity of a caprock. Both shaly OPA and carbonate-rich OPA are used for the investigation to assess the possible role of the mineralogical compositions. The higher carbonate content of the carbonate-rich OPA is supposed to trigger chemical reactions with CO_2 (carbonate dissolution) and result in more pronounced modification of the porous space than the shaly OPA. As explained in the next sections, different exposure methodologies are adopted for the two materials, to simulate different injection conditions.

The long-term chemical impact of acidic conditions on the material is also evaluated with an additional measurement of grain density after exposure to an HCl solution. Shaly OPA samples are exposed in an acidic environment at standard temperature and pressure for a 1 year. The impact on the material's grain density is presented and discussed later, together with the rest of the results.

3.3.1. Testing methodology

The general experimental procedure adopted for these tests is composed of three main phases: (i) the saturation of the sample with water and a final evaluation of the permeability, (ii) the exposure of the sample to CO_2, (iii) a final measurement of the permeability after the exposure. Compared to the short-term injection test presented in the previous section where the material is contact with CO_2 for some days, the injection of CO_2 in these long-term experiments is in the order of several weeks.

The permeability of a porous medium describes its aptitude to allow the circulation of a fluid throughout the porous space and depends on the internal porous structure and its connectivity. Thus, the triggering of chemical phenomena such as precipitation/dissolution in the presence of CO_2 would reflect in the material's permeability as a result of the porous space modification. The measurement of intrinsic permeability is performed with the constant head method (Darcy, 1856; Renard et al., 2001), applying a water pressure difference equal to 1 MPa between the upstream and downstream side of the sample. The permeability k (unit of m^2) of the medium can be calculated through the hydraulic conductivity K (unit m/s), considering the fluid's density ρ_f, the acceleration of gravity g and the fluid's dynamic viscosity η_f:

$$k = K \frac{\eta_f}{\rho_f \ g} \tag{2}$$

Based on the Darcy's law and neglecting the difference in elevation, the hydraulic conductivity can be calculated as follows:

$$K = q_f \frac{\rho_f \ g \ L}{A \ \Delta P_f} \tag{3}$$

where, q_f is the volumetric flow, L the height of the sample, A the area of the sample, ΔP_f the applied pressure difference.

3.3.2. Carbonate-rich OPA

Pre-exposure phase

The pre-exposure phase of the test is illustrated in Fig. 9. The carbonate-rich Opalinus Clay sample is also resaturated before the injection phase. The process is performed with distilled water under constant total axial stress. At both upstream and downstream sides a fluid pressure of 100 kPa is applied, while the total axial stress is kept constant at 450 kPa. During the process, the vertical axial displacement of the specimen is continuously monitored. The behaviour of the specimen stabilised after about one day since the start of the injection of water, with a total expansion of 13 μm that corresponds to an axial strain of 10×10^{-6} % (Fig. 10). This very low value of axial strain is expected given the fact that the high initial degree of saturation of the sample, while it could also indicate a lower sensitivity of the carbonate-rich Opalinus Clay to wetting. To further enhance the specimen's saturation the axial stress was increased to 2.1 MPa and the water pressure was raised to 1.0 MPa at both upstream and downstream sides.

After the sample's saturation, a series of loading and unloading steps between 2.1 MPa and 8.6 MPa of total axial stress is carried out in order to evaluate the permeability at different stress levels (see Fig. 9). The hydraulic conductivity is measured at each stress level according to the constant head method (similarly to the shaly OPA sample). The upstream water pressure is set to 1.5 MPa and the pressure at the downstream side to 0.5 MPa, resulting in a pressure difference of 1.0 MPa. As

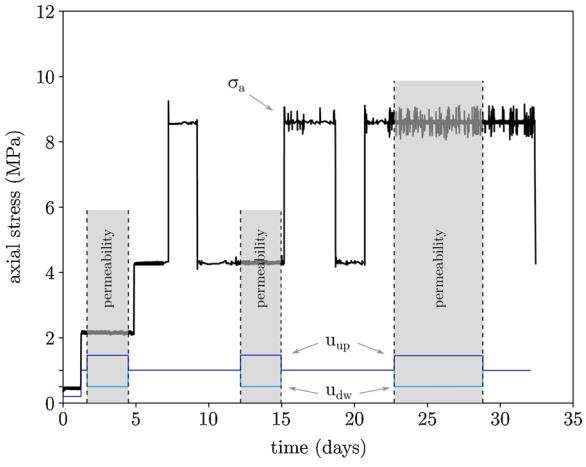

Fig. 9. Evolution of the total axial stress and pore pressure during the first phase of the test (saturation, permeability and consolidation) of the carbonate-rich OPA sample.

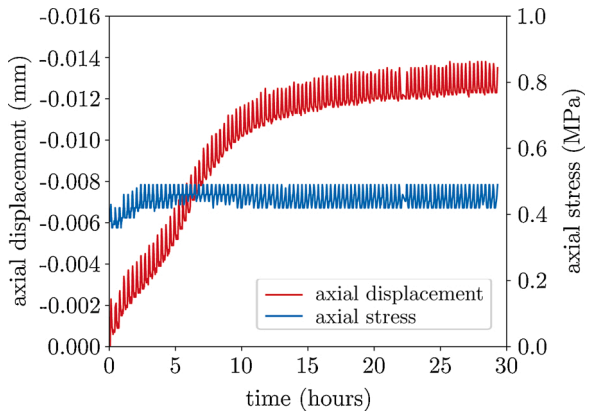

Fig. 10. Evolution in time of the displacement and axial stress during the initial saturation phase of the test.

presented in Fig. 9, a first permeability measurement takes place for a total axial stress of 2.1 MPa, corresponding to a void ratio equal to 0.091. The sample is then loaded to a total axial stress equal to 8.6 MPa in two steps, causing a reduction of the void ratio to 0.083. The second measurement of permeability is, however, performed after unloading the sample to a total axial stress equal to 4.3 MPa, corresponding to a void ratio equal to 0.084. This value is similar to the void ratio at 8.6 MPa of total axial stress due to the overconsolidated state of the material. The last permeability measurement is carried out at 8.6 MPa of total axial stress, corresponding to a porosity value equal to 0.082 The obtained permeability values are gathered and discussed in a later section.

CO_2-rich water injection

The CO_2 injection phase is started by injecting CO_2-rich water in the water saturated sample, which is subjected to a constant total axial stress of 4.3 MPa and an initial pore water pressure of 1.5 MPa (Fig. 11). The choice of using CO_2-rich water is made to consider a configuration similar to the *in-situ* experiment carried out in the Mont Terri laboratory presented in (Zappone et al., 2018). For this purpose, CO_2 is allowed to diffuse in a constant volume reservoir (placed outside the oedometric cell) filled with water that is connected to the upstream side of the sample. For the preparation of the CO_2-rich water, the reservoir is initially filled partially with 44 cm^3 of water, while the remaining volume (about 20 cm^3) is occupied by the injected CO_2. The amount of CO_2 that dissolves in the water depends on the applied to CO_2 pressure (1 and 1.5 MPa) and the corresponding solubility value, which is ranging between 0.40 mol/dm^3 and 0.55 mol/dm^3. Thus, the generated carbonated fluid (CO_2-rich water) is pushed towards the upstream side of the sample by the applied CO_2 pressure, as illustrated in Fig. 11. Except for comparison to the *in-situ* test conditions, the reason of this choice is related to the possibility of exposing the material to a higher amount of acidic fluid during the injection and better simulate the possibility of a fluid migration in the caprock.

During this first phase of the exposure, the CO_2-rich fluid is injected at the upstream side (P_{CO_2}) with a pressure of 1.5 MPa for 5.6 days. At the downstream side, a constant volume reservoir initially filled with distilled water is connected to the sample with an initial pressure (u_w^{dw}) of 1.0 MPa. The temperature is controlled at 23 ± 0.5 °C. During the injection, a gradual pressure build-up has been observed at the downstream side until its stabilisation to 1.5 MPa. Negligible deformations have been experienced by the sample during this time.

At the end of the treatment, the water pumps are back connected to both sides of the sample for the measurement of the permeability; similarly, flushing of the pore lines is required to replace the carbonated fluid with distilled water. An initial resaturation of the specimen is performed for 5.8 days with a water pressure at the upstream and downstream sides of 1.5 and 0.5 MPa, respectively. The permeability test is then conducted for 3 days, under a constant total axial stress of 4.3 MPa.

The second phase of the CO_2 exposure in the carbonate-rich OPA sample is launched immediately after the permeability measurement. The goal of this phase is to maximise the exposure of the sample to the acidic fluid by increasing the amount of fluid that flows in the pore space. This condition is representative of a situation where the caprock is not capable to behave as a barrier preventing the migration of CO_2. To achieve this goal the testing set-up is slightly modified from the previously presented tests. Indeed, in order increase the fluid flow in the material, a reservoir filled with water at atmospheric pressure is connected at the downstream side (P_w = atm). The reservoir includes a burette that allows the measurement of the outflow. This configuration allows the application of a constant pressure difference across the sample equal to 1 MPa throughout the entire injection phase of the test (Fig. 11), and it is capable to provide continuously fresh CO_2-rich fluid to the sample.

The temperature is controlled and maintained at 23 ± 0.5 °C during the injection, while the total axial stress is kept constant at 4.3 MPa. The injection of CO_2-rich water has lasted for 53 days, after which the permeability is once more measured.

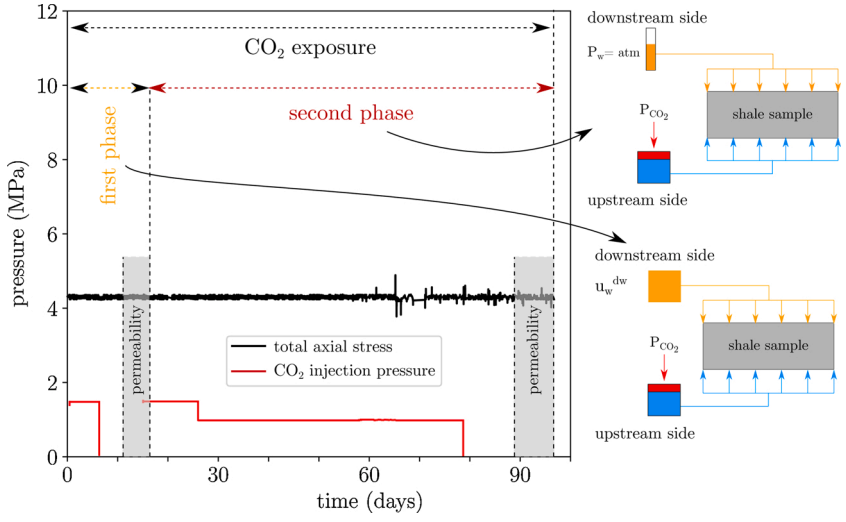

Fig. 11. Testing layout adopted for the long-term injection test performed on the carbonate-rich OPA sample.

3.3.3. Shaly OPA

Pre-exposure phase

The long-term injection test on the shaly OPA is performed at higher mechanical stress and fluid pressures compared to the test on the carbonate-rich OPA. Fig. 12 illustrates the evolution in time of the axial stress and the water pressure during the pre-exposure phase.

The initial loading of the sample to a total axial stress of 24 MPa is performed at constant water content (w = 3.7%) which induces a reduction of the void ratio from e = 0.202 to 0.179. Afterwards, the sample is put in contact with distilled water at a pressure of 100 kPa at both upstream and downstream sides for the resaturation in constant volume conditions. The axial stress is therefore progressively increased to limit sample's expansion while the water is slowly injected. Fig. 13 shows the evolution of the axial deformation experienced by the sample during the process, and the corresponding increase of the total axial stress that is applied in order to limit swelling. The process stabilises after about 1 day; a volumetric swelling of −0.097% is observed, along with an increase of the total axial stress by 3.5 MPa (from 24 MPa to 27.5 MPa). Next, the sample is loaded to a total axial stress equal to 30 MPa, and water pressure is increased to 8 MPa in order to achieve an effective axial stress equal to 22 MPa.

Before the injection CO_2, the sample's permeability is measured using a steady state method. A water pressure difference of 1 MPa is applied between the upstream and downstream sides, with a pressure of 8.5 MPa at the upstream side and 7.5 MPa at the downstream side; a constant total axial stress equal to 30 MPa is constantly applied during the measurement. The pressure difference is maintained constant for 2 days while the inflow and outflow are continuously monitored.

CO_2 injection phase

Fig. 4b illustrates the methodology adopted to carry out the CO_2 injection. CO_2 is injected in progressive steps at the upstream side, while at the downstream side the sample is connected to a constant volume reservoir filled with CO_2, where the pressure variation is monitored. This configuration is representative of an intact caprock, where the pore fluid is not supposed to migrate in the material along preferential pathways characterised by a higher permeability. Before starting the injection of CO_2, the pore lines upstream and downstream are flushed in order to remove the water and having the CO_2 directly in contact with the bases of the sample. Initially, a CO_2 pressure of 8 MPa is applied at both upstream and downstream sides to avoid changes of the back fluid pressure. Considering that the temperature during the test is in the range between 21 and 24 °C, the CO_2 is injected in a liquid phase. After this initial step, the CO_2 pressure at the upstream side is increased in six steps up to 16 MPa lasting for different duration periods as shown in Fig. 14. The pressure increase at each step is equal to either 1 or 2 MPa. The total axial stress is kept constant and equal to 30 MPa during the entire CO_2 injection phase that lasted 105 days.

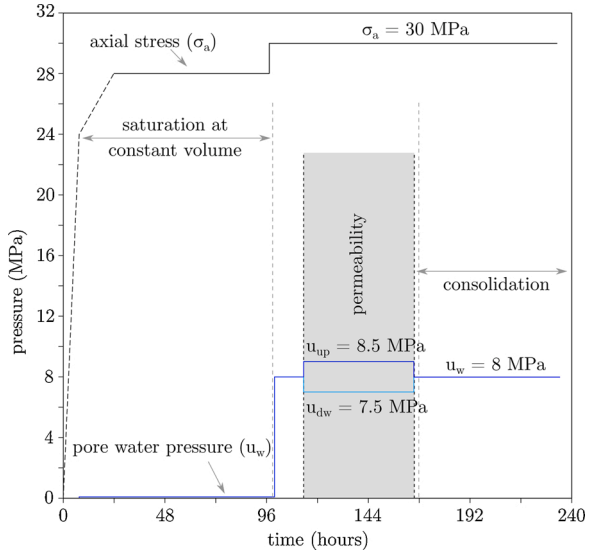

Fig. 12. Evolution of the total axial stress and fluid pressure during the pre-exposure phase (saturation, permeability and consolidation) of the long-term injection test performed on the shaly OPA sample.

4. Results

In this section, the different obtained results are presented, analysed and compared. First, the evaluation of the capillary entry-pressure is presented according to the results obtained from the short-term test performed on the shaly OPA, while the significance of the sample's initial saturation is highlighted. Afterwards, the analysis of the impact of chemical effects on permeability is presented, for both shaly and carbonate-rich OPA through the long-term injection tests. The impact on the material's pore size distribution (PSD) is finally evaluated, as well as the influence of the pore fluid pH on the material's grain density.

4.1. Capillary entry-pressure

The sealing capacity of the Opalinus Clay is first evaluated with the short-term injection test on the shaly OPA in terms of capillary entry-pressure. Fig. 15a summarises the hydraulic response of the sample, where the evolution of the CO_2 injection pressure in time at upstream side (red plot) and the recorded CO_2 pressure at the downstream side (orange plot) are illustrated. During the first step where the upstream CO_2 pressure is increased to 4 MPa, the pressure at the downstream side does not exhibit any variation, revealing the response of the material as perfect barrier capable to prevent the penetration and propagation of CO_2 throughout the sample. A slight increase of the downstream pressure is then observed during the second step, where the CO_2 injection pressure is increased to 8 MPa at the upstream side. This pressure increase in the downstream reservoir indicates that the capillary entry-pressure of the sample has been exceeded during this step, and the CO_2 has been able to penetrate and find a path across the sample to reach the downstream side. This response is confirmed in the third step, where the CO_2 pressure is further increased to 12 MPa, and the pressure increase at the downstream side is even more significant compared to the previous step. Finally, during the last step where the injection pressure is decreased back to 8 MPa, a reduction of the pressure increase at the downstream side is observed. Based on these outcomes, the capillary entry-pressure is identified during the second injection step, when the injection pressure has been increased from 4 to 8 MPa. The entry-pressure is measured as the pressure difference between the injected CO_2 pressure and the pore water pressure when an increase of CO_2 pressure is observed at the downstream side, thus, it is estimated to be within the range between 2 MPa and 6 MPa. The observed pressure increase at the downstream side cannot be related to a diffusive flow mechanism in such a short time period (Busch et al., 2008).

The mechanical response of the sample in terms of measured axial displacements is plotted in Fig. 15b, where positive displacement corresponds to compaction. A compaction is observed in each step where the CO_2 pressure at the upstream side is increased. At each step, a first instantaneous displacement is recorded corresponding to the increase of the CO_2 pressure, followed by a delayed response where the sample continues compacting at smaller rate. The existence of creep after the increase of the CO_2 injection pressure is confirmed during the initial step (Step 0) when looking at the response of the sample before and after the water replacement with CO_2 (at 2 MPa pressure). Fig. 16 shows the displacement exhibited by the sample during the consolidation stage to 24 MPa of total axial stress, followed by the response experienced after water is replaced by CO_2 (Step 0). The graph clearly proves that the observed response during the initial step of the injection is a continuation of the creep deformation already started at the end of the consolidation stage. A similar time-dependent response is also observed in the

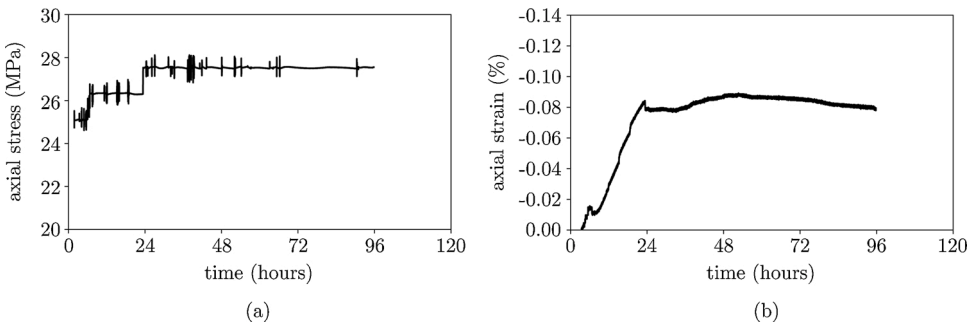

Fig. 13. Resaturation phase of the test: (a) swelling stress; (b) axial deformation.

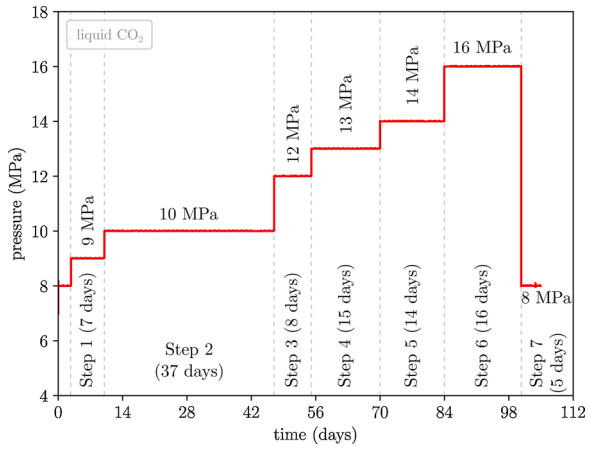

Fig. 14. Applied upstream CO_2 pressure during the long-term injection test.

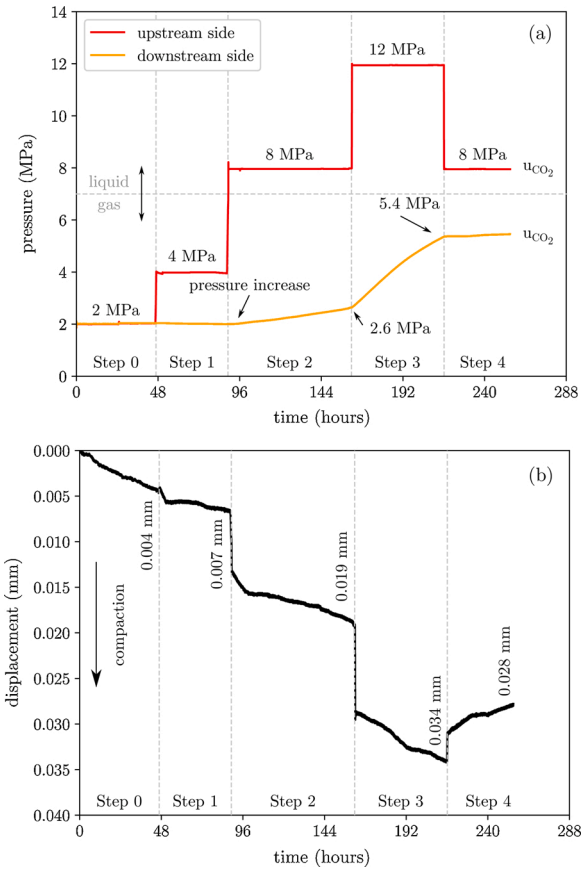

Fig. 15. Hydro-mechanical response of the shaly OPA sample during short-term injection of CO_2; (a) upstream and downstream pressure and (b) axial displacement with time. (For interpretation of the references to color in the text, the reader is referred to the web version of this article.).

following injection steps. However, in these cases, the role of consolidation should be taken into account due to the variation of the average pore fluid pressure induced bay the injection. This process can be analysed in shales when the sample is fully saturated with one fluid (Ferrari et al., 2016). Considering the difficulties in estimating the sample fluids saturation and the average pore fluid pressure during the performed test, a clear distinction between the end of the consolidation process and the start of creep deformations is not possible. Finally, in the last step where the CO_2 injection pressure is decreased to 8 MPa, an expansion of the sample is observed. This response is consistent with the one observed in the previous steps.

The observed hydro-mechanical response of the Opalinus Clay during the injection of CO_2 is significantly related to the development of capillary forces in the water saturated sample. Indeed, when a single fluid is present in the pore space of a geomaterial, an increase of the injection pressure of the same fluid is entirely transmitted to the fluid in the pore space, causing an expansion of the material due to a decrease of the effective stress. However, when two immiscible fluids are present in the pore space of the material, capillary forces develop at the interface between the two fluids, and the pressure increase of the injected fluid (CO_2) is not transmitted to the pore fluid (water). The capillary forces result in pulling the material's particles together leading to an overall compaction of the sample. A rough estimate of the capillary forces in geomaterials can be obtained with Young-Laplace equation, which relates the capillary pressure to the pore diameter and wettability with the assumption of a cylindrical capillary tube (Iglauer et al., 2015). In the case of the Opalinus Clay and more generally of shales, capillary forces may be significant (in the order of some MPa) due to their extremely small pore size (in the nanometer range as presented by the MIP results in Section 2). The impact of capillary forces on the mechanical response of the material during the injection of CO_2 is influenced by the CO_2/water saturation of the sample. For instance, if most of the pore space is occupied by CO_2, the overall average increase of the pore pressure in the material caused by the injection prevails on the effect induced by the presence of capillary forces.

Before the penetration of CO_2 in the sample (during the Step 1 with injection pressure equal to 4 MPa), the capillary forces only develop on the upstream boundary of the sample and they can perfectly sustain the CO_2 over-pressure causing a small compaction of the material; this capillary barrier system has been able to prevent the migration of CO_2 across the sample, and no pressure variations are observed at the downstream side. However, once the CO_2 is recovered at the downstream side (Step 2 where the injection pressure is increased to 8 MPa), the capillary forces start to develop also inside the sample along the pathways that convey the CO_2 across the material. This feature leads to a more pronounced compaction of the material in the second and third

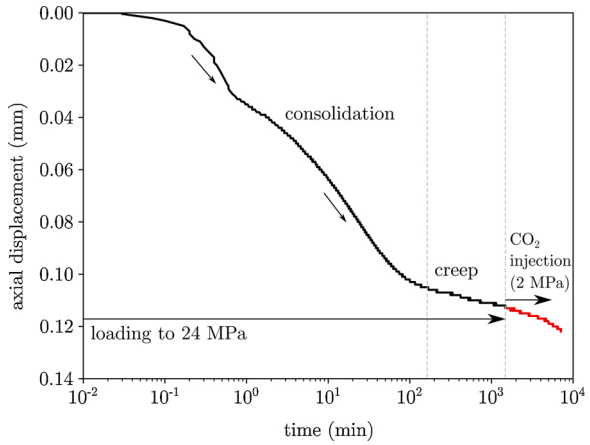

Fig. 16. Response of the sample during the consolidation stage along with the initial step of the CO_2 injection phase of the test where a CO_2 pressure equal to 2 MPa is applied to both upstream and downstream sides.

steps, where the injection pressure is increased to 8 and 12 MPa. The observed behaviour support the assumption that the CO_2 has been able to displace the water in the pore space and penetrate in the material just along localised pathways with lower water retention capabilities, leading to a partial desaturation of the sample. The mechanical behaviour observed in the last step (Step 5) when the injection pressure is decreased further supports this explanation. Indeed, the reduction of the CO_2 pressure induce a decrease of the capillary forces, which are responsible for the expansion experienced by the sample.

In order to further evaluate the importance of the initial saturation of the sample for the assessment of the sealing capacity, the short-term injection test is repeated on same shaly OPA sample after partial desaturation. Even though the caprock formation is expected to be fully saturated *in-situ*, the hydro-mechanical response of the desaturated material to CO_2 injection merits investigation itself; first in order to prove role of the capillary forces and fluid saturation on the variation of effective stress and then, to clarify the non-wetting fluid flow in the material (that is one of the remaining open key questions highlighted in Amann-Hildenbrand et al. (2015)).

In Fig. 17, the behaviour of the unsaturated shaly OPA sample is presented in terms of hydraulic and mechanical response. The comparison of Figs. 15a and 17 a reveal immediately the importance of an initial full saturation of the Opalinus Clay sample for a proper assessment of the material's entry-pressure. In the absence of the wetting fluid in the pore space, the injected CO_2 can directly penetrate through the material and reach easily the downstream side; few hours are sufficient for the pressure front to propagate across the entire unsaturated sample and equalise the entire system to the injection pressure.

In terms of mechanical response, Fig. 17b shows the evolution in time of the axial displacement for all the injection steps. The graph clearly illustrates that, when the material is not properly saturated with water, the injection of CO_2 induces an expansion of the sample. As the amount of water in the pore space is significantly lower compared to the amount of the injected CO_2, the impact of the capillary forces on the mechanical behaviour becomes secondary with respect to the overall average pore pressure increase with the increasing CO_2 injection pressure. These results clearly highlight that the water saturation of the sample does not only affect the sealing capacity of the material, but also for the mechanical response exhibited by the material during the injection of CO_2. The mechanical response of the two tests (saturated and unsaturated) suggests that the penetration of the CO_2 in the saturated material is not associated to an expansion response related to the generation of new pathways and fractures.

The results of the test carried out with the residual pressure method are finally presented for the assessment of the capillary entry-pressure.

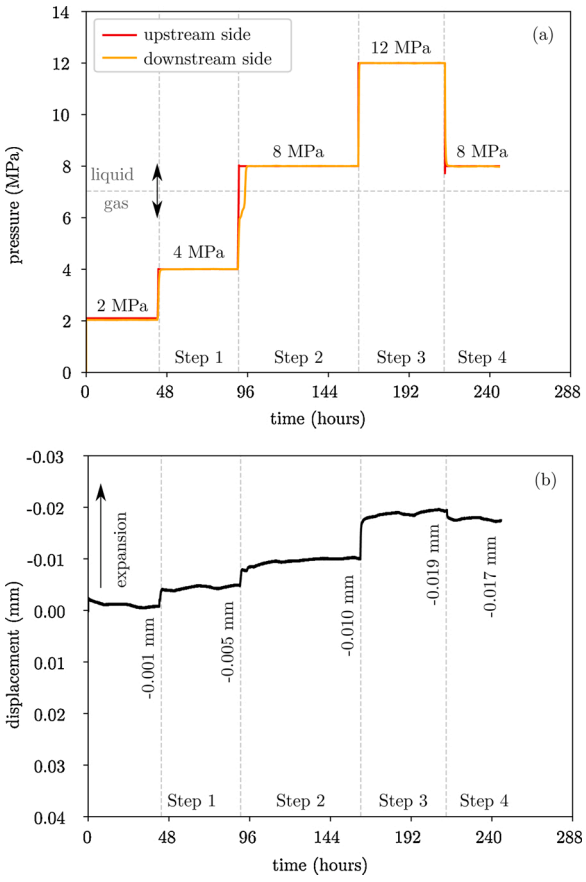

Fig. 17. Hydro-mechanical response in time of the unsaturated shaly OPA sample during short-term injection of CO_2; (a) upstream and downstream CO_2 pressure and (b) axial displacement.

The hydraulic response of the sample is presented in Fig. 18a, where the evolution of the CO_2 pressure at the upstream side and the water pressure at the downstream side is illustrated. After the sudden increase to 16 MPa, the pressure at the upstream side gradually decreases while at the downstream side a pressure increase is observed. These pressure variations indicate that the CO_2 penetrates in the sample and displaces the pore water towards the downstream reservoir. The pressure difference between the two sides stabilises to 3.5 MPa after 8 hours since the beginning of the injection, and it remains stable during the next 3 days. Direct comparison with the stepwise method is not appropriate, since different processes are occurring with each method; in the stepwise injection a wetting process takes place instead of the drying process occurring with the residual method.

Fig. 18b illustrates the mechanical response in terms of axial displacement experienced by the sample during the test. Initially, the instantaneous increase of the upstream pressure results in a rapid compaction of the sample. This response is similar to that observed in the short-term test performed with the stepwise method, where the development of the capillary forces is responsible for the compaction of the material. As the CO_2 moves progressively throughout the pore space towards the downstream side, the water is gradually displaced and pushed in the downstream reservoir, causing a consequent increase of the pressure and a local desaturation of the sample. This increase of pressure is then progressively transmitted to the water in the pore space that is responsible for a decrease of the capillary forces, which is further enhanced by the decrease of the CO_2 pressure in the upstream reservoir. As a consequence of this pressures evolution, the material exhibits an expansion response that stabilises once the capillary forces decrease to a value lower than the corresponding entry-pressure.

Finally, an estimation of the capillary entry-pressure from the MIP

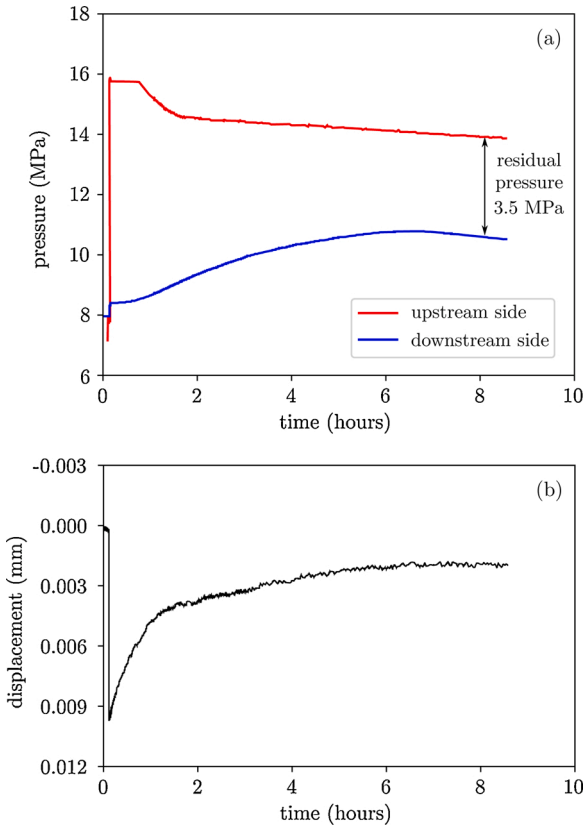

Fig. 18. Hydro-mechanical response in time of the shaly OPA sample according to the residual method; (a) upstream and downstream CO_2 pressure and (b) axial displacement.

test is also presented, based on the results presented in Fig. 2 for the shaly OPA. This methodology allows the preliminary and indirect evaluation of the sealing capacity of a low permeable material. However, several limitations have to be considered when used mercury intrusion data (Shafer and Neasham, 2000; Sigal, 2009; Comisky et al., 2011), and a proper and reliable assessment of the sealing capacity of a caprock material has to be performed with injection tests. In particular, the evaluation of the capillary entry-pressure has been performed according to the tangent method (Amann-Hildenbrand et al., 2015), taking into account the sample's surface roughness. The conversion of the pressure value from the mercury-air system to the CO_2-brine system has been carried out with the Washburn equation, considering the following values from literature for the interfacial tension (γ) and contact angle (θ): (i) Hg-air system $\gamma = 485$ mN/m and $\theta = 140°$ (Romero and Simms, 2008), (ii) CO_2-brine system $\gamma = 25$ mN/m and $\theta = 0°$, 30°, 60° (Bikkina, 2011). Depending on the contact angle adopted for the CO_2-brine system, the obtained capillary entry-pressure is in the range between 1.3 MPa and 2.7 MPa. Given the previously discussed limitations of this technique, the obtained values can be considered a lower limit of the entry-pressure of the tested material, and they support the validity of the results found from the stepwise injection test, as both methodologies are based on the evaluation of the capillary entry-pressure on a drainage path.

4.2. Impact on permeability

This section summarises the results of the long-term injection tests related to analysis of the chemical effect induced by the exposure of the material to CO_2. The results of the permeability tests performed on the carbonate-rich OPA are initially presented, followed by the outcomes on the shaly OPA.

4.2.1. Carbonate-rich OPA

The permeability of the carbonate-rich OPA sample is measured at different stages of the long-term test. The global overview of the different permeability measurements throughout the entire test is summarised in Fig. 19. First, three permeability measurements are performed before the CO_2 exposure under three different levels of axial stress. An intermediate measurement is carried out after the first phase (5.6 days), followed by a last evaluation at the end of the second phase (53 days). The second phase of the CO_2 exposure is designed to have the amount of injected carbonated fluid higher than the amount of initial water in the pore space, which is estimated to be equal to 1.42 ml. Fig. 20 shows the evolution of the monitored outflow volume in time that is collected at the downstream side during the entire injection period. The very low transport properties of the material are clearly highlighted, where more than 37 days are required in order to inject an amount of fluid equal to the void space of the sample. The injection then has further continued for a total time of 53 days, to increase the exposure time of the material to the acidic fluid.

At the end of both first and second phase of the CO_2 exposure, the water pumps are connected to the sample for the assessment of the permeability. Water pressures of 1.5 MPa and 0.5 MPa are applied at the upstream and downstream sides respectively, with a total axial stress of 4.3 MPa.

Fig. 21 presents a summary of all the permeability results obtained for this sample. The permeability values measured before the CO_2 exposure (grey points) highlight the dependency on the void ratio of the sample that is related to the corresponding applied total axial stress: the obtained values of permeability for the three stress levels (2.1, 4.3, and 8.6 MPa) are 7.5×10^{-20}, 3.4×10^{-20} and 2.6×10^{-20} m^2, respectively.

A small reduction of permeability is observed after the injection of CO_2. More precisely, the permeability after the first phase is measured equal to 2.6×10^{-20} m^2, while after second phase the permeability value is 2.1×10^{-20} m^2. The void ratio corresponding to the second permeability measurement is equal to 0.083, and it highlights the very small compaction experienced by the sample during the injection. The observed variations of permeability and void ratio before and after the injection are very small and can be considered within the accuracy of the adopted methodology. This aspect confirms the difficulties in quantifying such small porosity and permeability changes in shales. The graph includes also the permeability estimated during the second phase of the CO_2 exposure based on the outflow volume monitored at the downstream side with the burette (Fig. 20). A higher difference is observed in this case, where a significant lower value (5.9×10^{-21} m^2) is obtained. For this calculation, different viscosity and density values have been used considering the carbonated fluid instead of water. The values are obtained from the equation of state and experimental analysis reported by various authors; viscosity of CO_2 dissolved in water, $\mu = 0.9486$ μPa·s

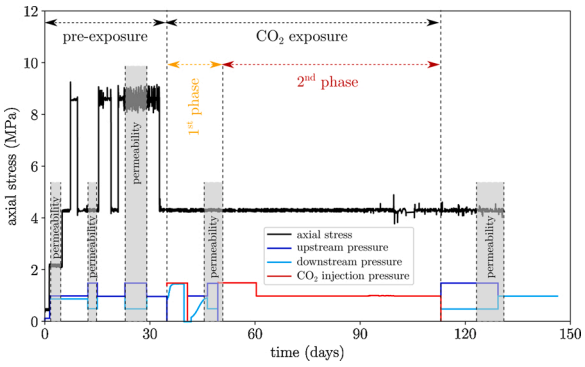

Fig. 19. Global overview of the test in terms of applied axial stress and fluid pressure, highlighting the performance of the different permeability measurements and the CO_2 exposure. (For interpretation of the references to color in the text, the reader is referred to the web version of this article.).

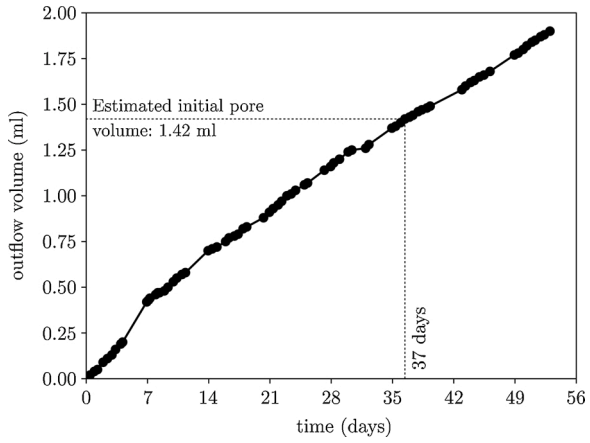

Fig. 20. Outflow volume measured at the downstream side during the second phase of the CO_2 exposure.

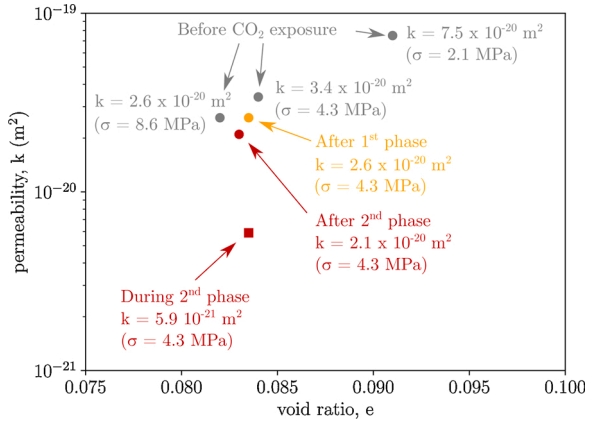

Fig. 21. Permeability values and void ratio of the carbonate-rich OPA sample measured during the different phases of the long-term injection test (together with the corresponding applied total axial stress).

and density of CO_2 dissolved in water, ρ_m =1.0062 g/cm^3 (Duan et al., 2006; McBride-Wright et al., 2015; Redlich and Kwong, 1949; Schmelzer et al., 2005).

In order to better investigate this aspect, an additional permeability assessment is performed using the same set-up adopted for the second phase of the CO_2 exposure, but injecting distilled water instead of the carbonated fluid. This further assessment is carried out to evaluate the possible impact of the different measuring systems at the downstream side (burette instead of the pump) on the obtained value of permeability. Distilled water is injected at 1 MPa at the upstream side, while atmospheric pressure is applied at the downstream side (burette exposed to free air). The fluid outflow at the downstream side is considered for the evaluation of the permeability. A value of 1.9×10^{-20} m^2 is obtained and it can be considered consistent with the value obtained using the constant head methodology for the same stress level (2.1×10^{-20} m^2). This result confirms that the different measuring system is not responsible for the observed variation of permeability. Thus, the reduction of permeability measured during the injection of the CO_2-rich fluid seems to be related to other physical mechanisms, related to the physical properties of the fluid (viscosity and density) and the interaction with the clay minerals (Busch et al., 2008). The overall outcomes of the analysis suggest that the injection of CO_2-rich fluid has not influenced significantly the permeability of the material for the given testing period and the amount of the supplied acidic fluid.

4.2.2. Shaly OPA

In the long-term injection test performed on the shaly OPA, permeability measurements are carried out before and after long-term CO_2 injection, under the same hydraulic conditions. The outflow volumes measured at the downstream side before and after the CO_2 injection are plotted in Fig. 22 for comparison. The two plots highlight a slightly lower flow after CO_2 exposure (0.0007 ml/h) compared to the flow before the injection (0.0010 ml/h). These outflow values lead to a small difference in terms of hydraulic conductivity, from 3.7×10^{-14} m/s (permeability, 3.7×10^{-21} m^2) before injection, to 2.6×10^{-14} m/s (permeability, 2.6×10^{-21} m^2) after injection.

As for the case of the carbonate-rich OPA, this permeability difference suggests a negligible impact of the CO_2 exposure for the given test duration (105 days) and the given CO_2 supply. In particular, the small decrease of the recorded outflow could be related to the presence of a residual CO_2 amount in the pore space of the sample, *i.e.* an incomplete water saturation of the sample. Consequently, a decrease of the void space available for the water to flow might have occurred. This aspect reveals the main challenge in this type of analysis, where the sensitivity of the transport properties of the Opalinus Clay to saturation changes could lead to misleading conclusions.

Compared to the long-term injection test performed on the carbonate-rich OPA where the carbonated fluid is directly injected, in this case the injected CO_2 can generated an acidic fluid just by reacting with the limited amount of water present in the pore space of the sample. Therefore, the amount of carbonated fluid that has been in contact with the material is smaller compared to the test carried out on the carbonate-rich OPA. This exposure methodology adopted for the shaly OPA better reproduce the real in-situ condition, where there is not any external source of carbonated fluid and the injected CO_2 can react only with the in-situ pore fluid.

4.3. Impact on structural properties

The pore structure of the shaly OPA sample after the long-term CO_2 injection test is investigated with Mercury Intrusion Porosimetry (MIP). The goal of this analysis is the evaluation of the possible impact of CO_2 exposure on the pore structure of the material.

The outcome of this last MIP test is then compared with the result already presented in Fig. 2a (that refers to the unexposed condition), and with the result presented in (Favero et al., 2018) where a shaly OPA sample was subjected to liquid CO_2 for 8.5 days. Fig. 23 compares these three MIP results. The grey curve corresponds to the sample that has not been exposed to CO_2, while the red (this study) and blue (Favero et al., 2018) curves show the results of CO_2 exposed material for comparison.

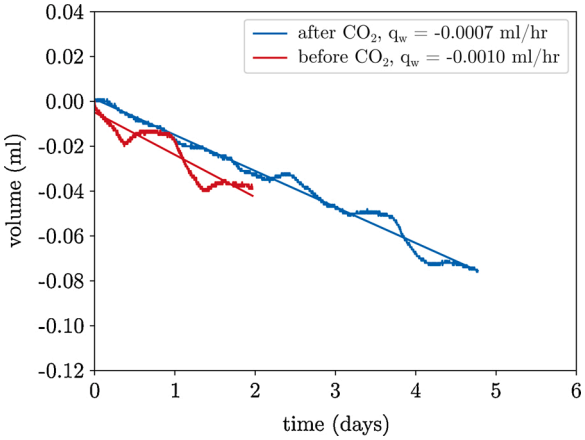

Fig. 22. Comparison of the measured outflow at the downstream side of the sample, during the permeability tests performed before and after CO_2 injection in the long-term test on the shaly OPA.

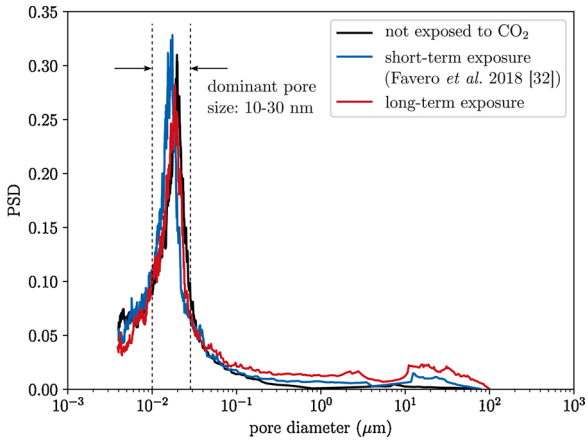

Fig. 23. Comparison of the pore size distribution of shaly OPA samples. (For interpretation of the references to color in the text, the reader is referred to the web version of this article.).

The obtained results do not highlight significant differences among the three results, meaning. Even though a slight shift of the peak towards a lower pore diameter is observed when the material is exposed to CO_2 injection, the dominant pore size remains limited between 10 and 30 nm. In addition, a slight difference can be observed in the higher range of pore diameter, between 10 μm and 100 μm. The specimens exposed to CO_2 seem to exhibit a slightly higher amount of pores in this size range. The observed variations are however very small and might be attributed to the accuracy of the MIP technique. Indeed, several limitations related to the detection of macro pores have to be considered when running MIP on shales, such as the Opalinus Clay, and they are mainly related to the presence of fissures and surface effects; an extensive review of these aspects can be found in Minardi (2018). According to this analysis, even the long-term exposure adopted in this study does not show significant alteration of the pore structure of the shaly ÕPA.

An additional evaluation of the possible impact of long-term exposure of the shaly material to an acidic fluid has been performed using a HCl solution in order to reproduce the pH values (3–4) typical of CO_2-rich fluids. Grain density measurements have been performed after different exposure periods under ambient temperature (22–24 °C) and in unstressed conditions using the water pycnometer technique. The obtained results have not highlighted any influence of the acidic fluid on the grain density, not even after one year of exposure.

5. Conclusions and perspectives

In the presented experimental study, the sealing capacity of the Opalinus Clay to CO_2 injection has been investigated through both short- and long-term injection tests, evaluating the hydro-mechanical behaviour and the possible impact of chemical effects on the material's permeability, pore size distribution, and grain density. Different experimental methodologies have been adopted to perform CO_2 (both gaseous and liquid) injection tests using a high-pressure oedometric cell to simulate the underground stress conditions. Two types of Opalinus Clay samples have been tested, aiming to investigate different aspects of the interaction between this shale formation and CO_2: a clay-rich (shaly facies) and a carbonate-rich (carbonate facies) core sample.

The sealing capacity of the shaly OPA has been investigated according to the stepwise injection and the residual method. The two methods involve different processes (drying and imbibition respectively) and yield information on the capillary entry-pressure and the snap-off pressure respectively. A capillary entry-pressure in the range between 2 and 6 MPa is obtained with the stepwise method, while a snap-off pressure equal to 3.5 MPa is obtained with the residual method. These results may be considered for off-shore storage analysis where CO_2 is injected in liquid phase, however, they are most probably over-assessed in comparison to super-critical conditions and thus, further testing is required for a more direct association to super-critical CO_2 storage. The role of the water saturation of the material on the evaluation of the capillary entry-pressure has been demonstrated with the results obtained from the short-term injection test carried out on the unsaturated Opalinus Clay.

The results of the injection tests have revealed important information in terms of mechanical behaviour. Indeed, a systematic compaction is experienced by the water saturated material when it is subjected to an increase of the CO_2 injection pressure. On the other hand, an opposite response (expansion) is observed when an increase of the CO_2 injection pressure is performed in the partially saturated Opalinus Clay. This hydro-mechanical behaviour is related to the development of capillary forces during the injection, and suggests that the CO_2 penetrates and propagates in the areas of the material with lower water retention capacity, without inducing any expansion of the material (generation of fissures and cracks) and causing a progressive desaturation as the injection pressure is increased. These outcomes highlight the importance of the water saturation of the material in assessing its sealing capacity and predicting the mechanical response during the injection of CO_2. Nevertheless, it is important to remind the significance of the caprock's wettability for the definition of its sealing capacity which decreases with increasing temperature. Therefore, the impact of temperature should be taken into account in future tests for CO_2 storage analysis.

The permeability analysis has not revealed a significant chemical impact of the material's exposure to CO_2. Both tested materials, carbonate-rich and shaly OPA, have not exhibited variations of permeability during the corresponding exposure periods of 58 days and 105 days, respectively. In particular, a slight decrease of permeability has been observed after CO_2 injection in both cases: from $3.7 \times 10^{-21}\,m^2$ to $2.6 \times 10^{-21}\,m^2$ for the shaly OPA, and from $3.4 \times 10^{-20}\,m^2$ to $2.1 \times 10^{-20}\,m^2$ for the carbonate-rich OPA. These reductions are extremely low, and might be attributed to the difficult resaturation of the material with water after the injection CO_2. This aspect highlights the sensitivity of the Opalinus Clay transport properties on the water saturation, which makes this type of analyses extremely challenging. Moreover, the different exposure methodologies adopted in the experiments, injecting either pure gaseous/liquid CO_2 or CO_2-rich water, have not played any role for the exposure periods investigated. However, a different permeability value ($5.9 \times 10^{-21}\,m^2$) is exhibited by the carbonate-rich OPA when the measurement is carried out directly during the injection of the CO_2-rich water rather than using distilled water. This outcome supports the role of sorption effects played by the clay particles when in contact with an acidic fluid already presented in the literature.

Finally, chemical effects related to CO_2 exposure have not been detected neither with the analysis of the pore size distribution performed with Mercury Intrusion Porosimetry test on the shaly OPA. In terms of grain density no variation has been observed after exposure of the material for one year to the HCl acid solution that used to simulate the pH condition generated by the reaction between CO_2 and water.

The experimental outcomes of the study provide an improved understanding of the hydro-mechanical behaviour of a shale caprock during CO_2 injection, and even though not directly representative of the super-critical *in-situ* underground conditions, they support the possibility of considering the Opalinus Clay formation as caprock for CO_2 storage. A significant capillary entry-pressure has been observed, along with a low sensitivity of the transport properties to CO_2 exposure for the analysed testing period. These features being fundamental requirements for the sealing capacity and the integrity of a caprock necessitate further investigation for a more direct association to the CO_2 storage field.

Author statement

Alberto Minardi: Designed and carried out experiments, analysed

experimental data, wrote, reviewed and edited the manuscript

Eleni Stavropoulou: Analysed and illustrated experimental results, wrote, reviewed and edited the manuscript

Taeheon Kim: Carried out and analysed carbonate-rich experiment, reviewed the manuscript

Alessio Ferrari: Supervised and reviewed the manuscript

Lyesse Laloui: Supervised and reviewed the manuscript

Conflict of interest

The authors declare no conflict of interest.

Acknowledgements

The European project ACT ELEGANCY, Project No 271498, has received funding from DETEC (CH), BMWi (DE), RVO (NL), Gassnova (NO), BEIS (UK), Gassco, Equinor and Total, and is co-funded by the European Commission under the Horizon 2020 programme, ACT Grant Agreement No. 691712. This project is supported by the pilot and demonstration programme of the Swiss Federal Office of Energy (SFOE). It is conducted within the Swiss Competence Center for Energy Research – Supply of Electricity (SCCER-SoE/Innosuisse).

The Authors would also like to thank Christophe Nussbaum and SwissTopo for contributing to the funding of this work and for providing the tested core samples from the Undeground Mont-Terri Laboratory, and Professor Martin Mazurek (University of Bern) for the mineralogical analyses performed on the tested materials.

References

Amann-Hildenbrand, A., Ghanizadeh, A., Krooss, B.M., 2012. Transport properties of unconventional gas systems. Mar. Pet. Geol. 31 (1), 90–99.
Amann-Hildenbrand, A., Krooss, B.M., Bertier, P., Busch, A., 2015. Laboratory testing procedure for CO2 capillary entry pressures on caprocks. In: Carbon Dioxide Capture for Storage in Deep Geological Formations, vol. 4, pp. 383–412.
Armitage, P.J., Faulkner, D.R., Worden, R.H., 2013. Caprock corrosion. Nature.
ASTM, D., 2010. Standard Test Methods for Specific Gravity of Soil Solids by Water Pycnometer, p. D854.
Bikkina, P.K., 2011. Contact angle measurements of CO2-water-quartz/calcite systems in the perspective of carbon sequestration. Int. J. Greenh. Gas Control 5 (5), 1259–1271.
Bossart, P., Thury, M., 2008. Mont Terri Rock Laboratory. Project, Programme 1996 to 2007 and Results. Wabern: Reports of the Swiss Geological Survey. Mont Terri Project, p. 3. Wabern Switzerland.
Boulin, P.F., Bretonnier, P., Vassil, V., Samouillet, A., Fleury, M., Lombard, J.M., 2013. Sealing efficiency of caprocks: experimental investigation of entry pressure measurement methods. Mar. Pet. Geol. 48, 20–30.
Busch, A., Müller, N., 2011. Determining CO2/brine relative permeability and capillary threshold pressures for reservoir rocks and caprocks: recommendations for development of standard laboratory protocols. Energy Proc. 4, 6053–6060.
Busch, A., Alles, S., Gensterblum, Y., Prinz, D., Dewhurst, D.N., Raven, M.D., Stanjek, H., Krooss, B.M., 2008. Carbon dioxide storage potential of shales. Int. J. Greenh. Gas Control 2 (3), 297–308.
Busch, A., Schweinar, K., Kampman, N., Coorn, A., Pipich, V., Feoktystov, A., Leu, L., Amann-Hildenbrand, A., Bertier, P., 2017. Determining the porosity of mudrocks using methodological pluralism. Geol. Soci. Lond. Spec. Publ. 454 (1), 15–38.
Chevalier, G., Diamond, L.W., Leu, W., 2010. Potential for deep geological sequestration of CO2 in Switzerland: a first appraisal. Swiss J. Geosci. 103 (3), 427–455.
Chiquet, P., Broseta, D., Thibeau, S., 2007a. Wettability alteration of caprock minerals by carbon dioxide. Geofluids 7 (2), 112–122.
Chiquet, P., Daridon, J.L., Broseta, D., Thibeau, S., 2007b. CO2/water interfacial tensions under pressure and temperature conditions of CO2 geological storage. Energy Convers. Manag. 48 (3), 736–744.
Comisky, J.T., Santiago, M., McCollom, B., Buddhala, A., Newsham, K.E., 2011. Sample size effects on the application of mercury injection capillary pressure for determining the storage capacity of tight gas and oil shales. Canadian Unconventional Resources Conference.
Crisci, E., Ferrari, A., Giger, S.B., Laloui, L., 2019. Hydro-mechanical behaviour of shallow Opalinus Clay shale. Eng. Geol. 251, 214–227.
Darcy, H.P.G., 1856. Les Fontaines publiques de la ville de Dijon. In: Exposition et application des principes à suivre et des formules à employer dans les questions de distribution d'eau, etc. V. Dalamont.
Duan, Z., Sun, R., Zhu, C., Chou, I.M., 2006. An improved model for the calculation of CO_2 and solubility in aqueous solutions containing Na+, K+, Ca2+, Mg2+, Cl-, and SO42-. Mar. Chem. 98 (2–4), 131–139.
Egermann, P., Lombard, J.M., Bretonnier, P., 2006. A fast and accurate method to measure threshold capillary pressure of caprocks under representative conditions. SCA A 46.
Espinoza, D.N., Santamarina, J.C., 2017. CO2 breakthrough – caprock sealing efficiency and integrity for carbon geological storage. Int. J. Greenh. Gas Control 66, 218–229.
Favero, V., Laloui, L., 2018. Impact of CO2 injection on the hydro-mechanical behaviour of a clay-rich caprock. Int. J. Greenh. Gas Control 71, 133–141.
Favero, V., Ferrari, A., Laloui, L., 2016a. Thermo-mechanical volume change behaviour of Opalinus Clay. Int. J. Rock Mech. Min. Sci. 90, 15–25.
Favero, V., Ferrari, A., Laloui, L., 2016b. On the hydro-mechanical behaviour of remoulded and natural Opalinus Clay shale. Eng. Geol. 208, 128–135.
Favero, V., Ferrari, A., Laloui, L., 2018. Anisotropic behaviour of Opalinus Clay through consolidated and drained triaxial testing in saturated conditions. Rock Mech. Rock Eng. 51 (5), 1305–1319.
Ferrari, A., Favero, V., Marschall, P., Laloui, L., 2014. Experimental analysis of the water retention behaviour of shales. Int. J. Rock Mech. Min. Sci. 72, 61–70.
Ferrari, A., Favero, V., Laloui, L., 2016. One-dimensional compression and consolidation of shales. Int. J. Rock Mech. Min. Sci. 88, 286–300.
Hansen, O., Gilding, D., Nazarian, B., Osdal, B., Ringrose, P., Kristoffersen, J.B., Eiken, O., Hansen, H., 2013. Snøhvit: the history of injecting and storing 1 Mt CO2 in the fluvial Tubåen Fm. Energy Proc. 37, 3565–3573.
Hesse, M.A., Orr, F.M., Tchelepi, H.A., 2008. Gravity currents with residual trapping. J. Fluid Mech. 611, 35–60.
Iglauer, S., Al-Yaseri, A.Z., Rezaee, R., Lebedev, M., 2015. CO2 wettability of caprocks: implications for structural storage capacity and containment security. Geophys. Res. Lett. 42 (21), 9279–9284.
Kaveh, N.S., Barnhoorn, A., Wolf, K.H., 2016. Wettability evaluation of silty shale caprocks for CO2 storage. Int. J. Greenh. Gas Control 49, 425–435.
Makhnenko, R.Y., Vilarrasa, V., Mylnikov, D., Laloui, L., 2017. hydro-mechanical aspects of CO2 breakthrough into clay-rich caprock. Energy Proc. 114, 3219–3228.
Marschall, P., Horseman, S., Gimmi, T., 2005. Characterisation of gas transport properties of the Opalinus Clay, a potential host rock formation for radioactive waste disposal. Oil Gas Sci. Technol. 60 (1), 121–139.
McBride-Wright, M., Maitland, G.C., Trusler, J.M., 2015. Viscosity and density of aqueous solutions of carbon dioxide at temperatures from (274 to 449) K and at pressures up to 100 MPa. J. Chem. Eng. Data 60 (1), 171–180.
McCoy, S.T., Rubin, E.S., 2008. An engineering-economic model of pipeline transport of CO2 with application to carbon capture and storage. Int. J. Greenh. Gas Control 2 (2), 219–229.
Minardi, A., Crisci, E., Ferrari, A., Laloui, L., 2016. Anisotropic volumetric behaviour of Opalinus Clay shale upon suction variation. Géotech. Lett. 6 (2), 144–148.
Minardi, A., 2018. Hydro-mechanical characterization of gas shales and Opalinus Clay shale in partially saturated conditions. EPFL 8315.
Orellana, L.F., Scuderi, M.M., Collettini, C., Violay, M., 2018. Frictional properties of Opalinus Clay: implications for nuclear waste storage. J. Geophys. Res.: Solid Earth 123 (1), 157–175.
Palandri, J.L., Kharaka, Y.K., 2004. A Compilation of Rate Parameters of Water-Mineral Interaction Kinetics for Application to Geochemical Modeling (No. OPEN-FILE-2004-1068). Geological Survey Menlo Park CA.
Pendland, C.H., 2010. Measurements of Non-wetting Phase Trapping in Porous Media. Imperial College London, London, p. 154.
Redlich, O., Kwong, J.N., 1949. On the thermodynamics of solutions. V. An equation of state, Fugacities of gaseous solutions. Chem. Rev. 44 (1), 233–244.
Renard, P., Genty, A., Stauffer, F., 2001. Laboratory determination of the full permeability tensor. J. Geophys. Res.: Solid Earth 106 (B11), 26443–26452.
Rieke, H.H., Chilingarian, G.V., 1974. Compaction of Argillaceous Sediments. Elsevier.
Romero, E., Simms, P.H., 2008. Microstructure investigation in unsaturated soils: a review with special attention to contribution of mercury intrusion porosimetry and environmental scanning electron microscopy. Geotech. Geol. Eng. 26 (6), 705–727.
Rosenbauer, R.J., Koksalan, T., Palandri, J.L., 2005. Experimental investigation of CO2-brine-rock interactions at elevated temperature and pressure: implications for CO2 sequestration in deep-saline aquifers. Fuel Process. Technol. 86 (14-15), 1581–1597.
Salager, S., François, B., Nuth, M., Laloui, L., 2013. Constitutive analysis of the mechanical anisotropy of Opalinus Clay. Acta Geotech. 8 (2), 137–154.
Schmelzer, J.W., Zanotto, E.D., Fokin, V.M., 2005. Pressure dependence of viscosity. J. Chem. Phys. 122 (7), 074511.
Shafer, J., Neasham, J., 2000. Mercury porosimetry protocol for rapid determination of petrophysical and reservoir quality properties. In: International Symposium of the Society of Core Analysts. Fredericton. New Brunswick, Canada: Society for Core Analysts (2000, October), pp. 18–22.
Sigal, R.F., 2009. A methodology for blank and conformance corrections for high pressure mercury porosimetry. Meas. Sci. Technol. 20 (4), 045108.
Vilarrasa, V., Silva, O., Carrera, J., Olivella, S., 2013. Liquid CO2 injection for geological storage in deep saline aquifers. Int. J. Greenh. Gas Control 14, 84–96.
Wollenweber, J., Alles, S., Busch, A., Krooss, B.M., Stanjek, H., Littke, R., 2010. Experimental investigation of the CO2 sealing efficiency of caprocks. Int. J. Greenh. Gas Control 4 (2), 231–241.
Zappone, A., Rinaldi, A.P., Grab, M., Obermann, A., Claudio, M., Nussbaum, C., Wiemer, S., 2018. CO2 sequestration: studying caprock and fault sealing integrity. The CS-D experiment in Mont Terri. In: Fifth CO2 Geological Storage Workshop (vol. 2018, No. 1, 1–5). European Association of Geoscientists and Engineers (2018, November).
Zweigel, P., Lindeberg, E., Moen, A., Wessel-Berg, D., 2004. Towards a methodology for top seal efficacy assessment for underground CO2 storage. In: 7th International Conference on Greenhouse Gas Control Technologies. 5e9. September, Vancouver, Canada.